Colloid and Polymer Science
https://doi.org/10.1007/s00396-021-04883-w

ORIGINAL CONTRIBUTION

Tunable safranine T release from LbL films of single/blend polyanions

Dilara Yılmaz Aykut[1] · Öznur Yolaçan[1] · Hasine Kaşgöz[1] · Huseyin Deligoz[1]

Received: 14 February 2021 / Revised: 4 August 2021 / Accepted: 9 August 2021
© The Author(s), under exclusive licence to Springer-Verlag GmbH Germany, part of Springer Nature 2021

Abstract
Loading and release behavior of a cationic dye, namely, safranine-T, through layer-by-layer (LbL) multilayered films of poly(diallyldimethylammonium chloride) (PDADMAC) and single/blend anionic polyelectrolytes (PEs), namely, poly(acrylic acid) (PAA), and poly(styrenesulfonate) (PSS), are described. The growths of PDADMAC/PSS-PAA multilayers and their safranine-T sorption behavior are monitored using the UV–Vis technique and discussed in terms of blend composition of anionic PEs and pH as well as their hydrophilicity and topography. The dye loading and desorption properties of the LbL films prepared from single/blend negatively charged PEs mainly depend on the interactions of PEs and safranine T. Strong interactions between PSS and safranine T result in a higher dye entrapping inside LbL films whereas either PAA-rich or single PAA-based LbL film exhibits larger dye desorption. A higher PSS content in the feed blend composition leads to an observable increase in θ_{ave} and surface roughness whereas the use of PAA can yield a flatter surface due to its partially recomposed chain conformational structure at pH 11. Consequently, LbL multilayers obtained from single and blend polyanions can be considered as an encouraging material platform for the controlled release of charged species such as protein, drug, and dye. because of their tunable physicochemical and morphological properties as well as surface wettability.

Keywords Adsorption · Desorption · LbL · Multilayer · Safranine-T

Introduction

Layer-by-Layer (LbL) assembly is a widely used technique to develop functional thin films [1–6]. The physicochemical properties of LbL films can be controlled by altering some parameters such as pH, temperature, ionic strength, salt composition, and charge density of the polyelectrolytes (PEs) [3, 7–11]. Because of these tunable properties, they are often preferred for applications where ultrathin functional films are required [12–15]. In addition to electrostatically interacted LbL films [16–20], hydrogen bonds, covalent bonds, van der Waals, hydrophobic, host–guest, and bio-specific interactions contribute to the fabrication of LbL films [21–24].

In literature, various thin-film applications including drug delivery [25–29], biosensor [30–33], membrane separation [34], actuators [35–37], catalysis [38–40], tissue engineering [41–43], regenerative medicine [44, 45], dye adsorption [46–52], and controlled drug/dye release [53–56] were presented. Among these applications, the sorption studies of stimuli-sensitive molecules through the LbL multilayer films received particular attention. These stimuli can be chemicals such as pH, ionic strength, or physical such as temperature [57–61]. Möhwald et al. pioneered the use of fluorescein kind of dye for the loading and release into/from LbL multilayered films [9]. In this study, an innovative polyelectrolyte multilayer (PEM) shell platform with controllable release characteristics was developed. They demonstrated that PEM shells assembled around cores of low molecular weight compounds can act as a barrier for release. In another study by Hammond and co-workers, they developed LbL thin films of positively charged poly(β-amino ester) and a series of model therapeutic polysaccharides (heparin, low molecular weight heparin, and chondroitin sulfate) for drug delivery and biomedicine applications owing to their biodegradability, pH dependency, and release behavior [29]. In another study by Feng and co-workers, methylene blue (MB) was loaded as a model dye onto/into LbL multilayered polyurethane (PU)/polyacrylic acid (PAA) films, and then the controlled release properties of this film were described. They illustrated that the pH of the MB solution had a significant effect

✉ Huseyin Deligoz
hdeligoz@istanbul.edu.tr

[1] Engineering Faculty, Chemical Engineering Dept, Istanbul University-Cerrahpaşa, 34320 Avcılar, Istanbul, Turkey

Published online: 02 September 2021

on adsorption, and the deposited MB amount increased with pH changing from 3 to 7 [62]. This report also showed that the release rate of MB can be controlled by the ionic strength and pH of the releasing medium. Lutkenhaus and co-workers produced hydrophilic polyethylene terephthalate (PET) fabric with adjustable surface properties using the LbL surface modification technique. According to this study, the coloration of PEM deposited on PET fabrics highly depended on both the surface properties of the fabrics and the physical properties of the dye [46].

Even if the topic of the article is popular and was widely investigated, the loading and release of safranine T through PDADMAC-PSS/PAA LbL films of single/blend polyanions were not reported so far. In this study, sorption behavior of a positively charged small model molecule (350.85 $g \cdot mol^{-1}$) through LbL multilayer films obtained from PDADMAC and single/blend PSS/PAA was described as a function of blend composition and pH. Blend structured films of polyanions were intentionally selected for the sorption studies since our previous study showed that PDADMAC/PSS-PAA films had a high loading capacity of small charged species [63]. Moreover, widely available, and economic cationic dye, namely, safranine T, was selected as the model molecule for the examination of interactions of the positively charged molecule and LbL multilayered film depending on pH and blend composition of polyanions. Furthermore, the growth, wettability, and surface topography of the LbL films from single/blend negatively charged PEs were studied.

Experimental section

Materials

Poly(styrenesulfonate) (PSS, Mw: 70,000 g/mol) and safranine T (Mw: 350.8 g/mol purity ≥ 85%) were supplied from Sigma-Aldrich. Poly(diallyldimethylammonium chloride) (PDADMAC, Mw:240,000 g/mol) and poly(acrylic acid) (PAA, Mw: 450,000 g/mol) were purchased from Polyscience. Structures of PDADMAC, PAA, and PSS are shown in Fig. 1. Ammonium hydroxide (26%) and sulfuric acid (95–97%) were obtained from Riedel-de Haën. NaCl (purity ≥ 99%), hydrogen peroxide (34.5–36.5% solution), sodium hydroxide, hydrochloric acid 37%, potassium chloride, monobasic potassium phosphate, sodium phosphate dibasic, 2-propanol (purity ≥ 99.8%), methanol (purity ≥ 99.9%), toluene (purity ≥ 99.9%), and 3-aminopropyl(diethoxy)methylsilane were received from Sigma-Aldrich. All chemicals were used without further purification. Nitrogen gas (purity ≥ 99.9%) was supplied from Linde Industrial Gases. Milli-Q-water ($R = 18.2$ MΩ) was used for all LbL deposition experiments.

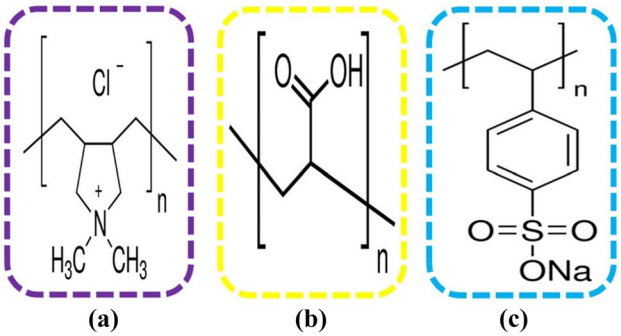

Fig. 1 Chemical structures of (**a**) PDADMAC, (**b**) PAA, and (**c**) PSS sodium salt

Methods

Preparation of PE solutions

In this study, the parameters obtained in our former works on the preparation of uniform LbL multilayered films were used [15, 63–66]. In this respect, PDADMAC and either PAA or PSS, or a mixture of PAA and PSS, were prepared at a concentration of 10^{-2} molar. The pH values of PDADMAC, PAA, and PSS solutions were 5.5, 1.8, and 1.8, respectively, and they were adjusted by adding diluted HCl or NaOH. Multilayers from single anionic PEs were abbreviated as $(PDADMAC/PAA)_n$ or $(PDADMAC/PSS)_n$; n is the number of deposited bilayers. LbL films of polyanions were constructed using PAA and PSS solutions in different compositions (75:25, 50:50, and 25:75). $(PDADMAC/PAA50PSS50)_n$ shows the LbL multilayered film obtained from PDADMAC and PAA/PSS blend in 50/50 (v/v) composition.

Fabrication of LbL multilayered films

Quartz glasses (quartz supports; Suprasil, Hellma GmbH, Germany) were used in the preparation and characterization of the LbL assembled films of single/blend negatively charged PEs. The quartz glasses were firstly cleaned according to the procedure reported formerly [67]. The quartz glass was then immersed into the positively charged PE solution for 10 min, followed by a rinsing step in ultrapure Milli-Q water for 5 min. Subsequently, it was immersed into the negatively charged single or blend PE solutions for 10 min, followed by washing with ultrapure water to remove the unbound or weakly attached PEs. This cycle continued until the completion of 20 bilayers on the quartz support, and these LbL films were characterized using the UV–Vis spectroscopy, contact angle tensiometer, and atomic force microscopy (AFM).

Dye adsorption and release from LbL multilayers

A schematic representation of the applied procedure is presented in Scheme 1. Dye adsorption through PDADMAC/PSS-PAA films was performed at pH 6.8 owing to their high loading capacity of small charged species without multilayer degradation reported in our recent article [15]. Similarly, pH 11 was chosen for desorption studies due to the stability of multilayer integrity of PDADMAC/PSS-PAA films from single/blend polyanions at this pH. Dye adsorption and release studies were performed according to the following procedure. LbL films of single or blend negatively charged PEs on quartz supports were initially immersed into phosphate buffer saline (PBS) containing safranine-T (0.5 g/L, pH:6.8) and kept in this solution for 24 h. After washing several times with PBS, the loading of safranine-T was characterized by UV–Vis spectroscopy, and the loaded amount of safranine-T was determined using the equation as follows:

$$\text{Loaded amount of safranine} - \text{T}\left({}^{ng}/_{cm^2}\right) = \left(C_0 - C_{24}\right) \times M_w$$

where C_0 and C_{24} are the initial concentration and the concentration after safranine-T adsorption at 24 h, respectively. M_w: molecular weight of safranine-T (g/mol).

The dye concentration was calculated using the UV absorbance (A) values of safranine-T at 518 nm as follows:

$$c = \frac{A}{\varepsilon . l}$$

where ε is the molar extinction coefficient (L mol^{-1} cm^{-1}) at 518 nm, and l is the path length.

For the release experiments, the dye-loaded LbL films of single or blend anionic PEs were immersed into 50 mL of PBS solution (pH:11). Release % of safranine-T through the LbL films was determined using the equation given as follows:

Release $\% = \frac{C_{loaded-Ct}}{C_{loaded}} \times 100$ where C_{loaded} is the concentration of safranine T deposited and C_t is the concentration of safranine-T released from the film at any time (t). The concentrations were found from the calibration curves with 0.9901 and 0.9959 regression coefficients for safranine-T loading at pH:6.8 and safranine-T desorption at pH:11, respectively.

The whole procedure employed in the study is shown in Scheme 1.

Analysis

UV – Visible (UV – Vis) spectroscopy measurements

Growth of the LbL multilayers and adsorption/desorption studies was followed using Perkin-Elmer Lambda 35 spectrometer with an integrating sphere unit. UV–Vis analyses were performed in the wavelength range of 190–600 nm. Before the deposition, the glasses were cleaned with Piranha solution (70:30 v/v solution of 97% sulfuric acid 30% hydrogen peroxide) as reported in the literature [60, 68, 69], and they were subsequently treated with 3-aminopropylmethyldiethoxysilane solution. The quartz glasses were dried with a weak stream of nitrogen before UV–Vis measurements. Caution: Piranha solution is highly corrosive. Extreme care should be taken when handling piranha solutions and only small quantities should be prepared.

Contact angle measurements

Surface hydrophilicity of the dye desorbed LbL films obtained from single/blend anionic PEs was determined by KSV Attension THETA optical contact angle device. Five microliters of ultra-pure water was dropped on the surface, and subsequently, the photos of drops were taken. The average contact angle (θ_{ave}) was reported with standard deviation after at least 3 repeated measurements.

AFM measurements

Surface topographies of the dye desorbed LbL films obtained from single/blend negatively charged PEs were characterized by atomic force microscopy (AFM Bruker Dimension icon device and Bruker's own type RTESP MPP-11100–10, $k = 40$ N/m, Bruker AXS). The root-mean-square (rms) values were calculated from 2 μm × 2 μm or 0.5 μm × 0.5 μm scanned areas on the substrates with 1 Hz scan rate, 512 samples/line. The NanoScope analysis 1.5 program was used to export the roughing account and the pictures.

Results and discussion

UV–Vis analysis of multilayer formation

Multilayer growths of the LbL assembled film of single/blend anionic PEs were followed using the UV–Vis technique as well as their safranine T sorption properties. For the monitoring of multilayer building-up of the LbL films, the UV–Vis absorption peak at 226 nm corresponding to the characteristic peak of PSS was followed [63]. To better understand the growth of the multilayers, UV–Vis graphs for $(\text{PDADMAC/PSS})_{20}$ and $(\text{PDADMAC/PSS50PAA50})_{20}$ are given in Fig. 2. As one can see from the figure, the multilayer adsorption of PDADMAC/PSS exhibited a slight exponential increase with the number of deposited bilayers while (PDADMAC/PSS50PAA50) displayed a relatively linear change in adsorption until fifteen bilayers. As it was known from the literature, the multilayer growth can occur linearly or exponentially depending on various factors such as charge

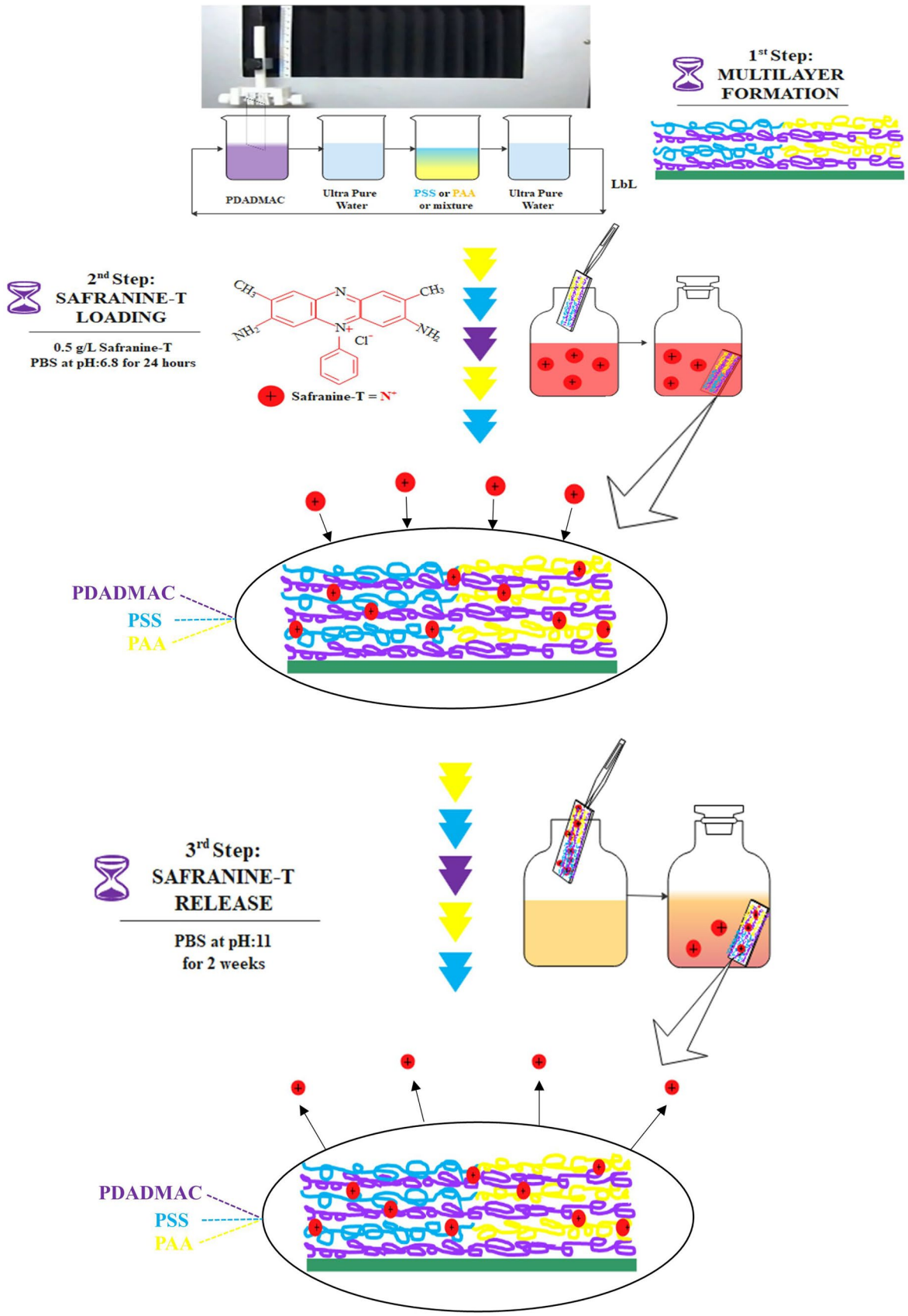

Scheme 1 A schematic representation of the LbL multilayer film deposition, safranine-T loading, and desorption

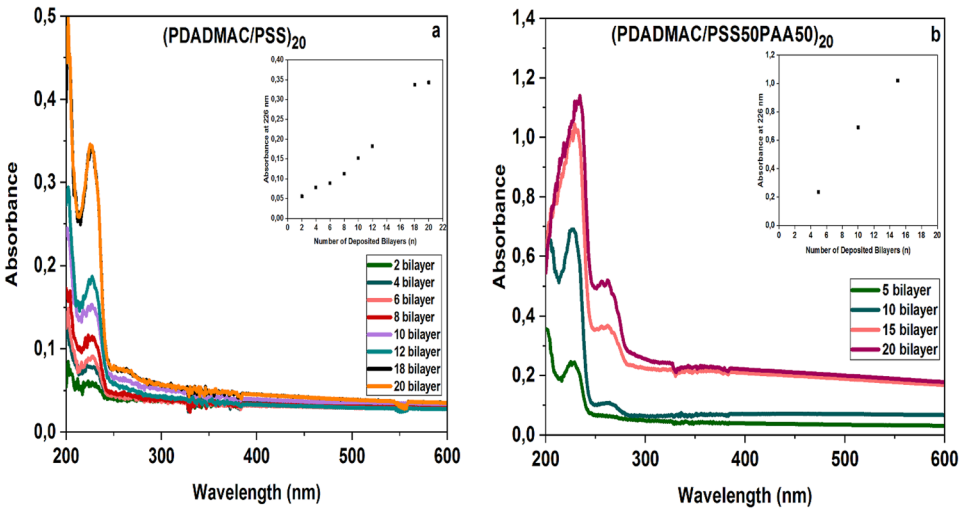

Fig. 2 UV absorbances of (**a**) $(PDADMAC/PSS)_{20}$ and (**b**) $(PDADMAC/PSS50PAA50)_{20}$ as a function of the number of deposited bilayers

density of PEs and external salt addition [59]. Also, the use of blended polyanions can lead to a change in multilayer growth probably due to the variation of ionic strength and charge density [70]. High absorbance values revealed a large accumulation of the multilayers on the substrate [63]. For comparison, smaller absorbances for $(PDADMAC/PSS)_{20}$ implied less multilayer accumulation possibly due to the high charge density of PSS and its high protonation at pH 1.8. In that case, a less amount of PSS will be sufficient to compensate for the positive charges of PDADMAC. The large accumulation of $(PDADMAC/PSS50PAA50)_{20}$ can be explained by the existence of PAA in the film composition because PAA, which is a weak PE, can largely deposit on the support to balance positive charges of PDADMAC. Another reason may be the loopy conformation of PAA. On the other hand, the films of $(PDADMAC/PSS50PAA50)_{20}$ showed a bit of shoulder in the range of 250–300 nm. These peaks may correspond to PAA existence, and this result is well consistent with the literature [63, 71].

In vitro studies of dye adsorption/desorption

The sorption behavior of a positively charged small molecule, namely, safranine T, through LbL film was investigated in terms of blend composition of polyanions, pH, and time. safranine T loading and release% of the LbL multilayered films depending on these conditions are presented in Table 1.

Concerning safranine T loading into/onto the LbL multilayered films of single/blend anionic PEs, safranine T loadings were in the range of 317.2 mg/cm^2 and 3960.8 mg/cm^2. safranine T depositions through $(PDADMAC/PAA)_{20}$ and $(PDADMAC/PSS)_{20}$ were found to be 317.2 and 435.5 mg/cm^2, respectively. This relatively high safranine T adsorption for $(PDADMAC/PSS)_{20}$ can mainly correspond to the stronger interactions of PSS and cationic dye at pH:6.8. At loading pH, the reaction of unprotonated sulfonic acid groups with the amino groups of safranine T can take place due to partly protonation of PSS. A proposed mechanism showing safranine T loading or desorption is given in Scheme 2 a and b. On the other hand, $(PDADMAC/PAA)_{20}$ was mostly deprotonated at pH:6.8 due to the weak PE character of PAA, and it can give a reaction between carboxylic acid of PAA and amino groups of the dye. For comparison with our previous study, cationic dye adsorption was found to be smaller than that of ibuprofen sodium salt (IBF-Na) loading for $(PDADMAC/PAA)_{20}$ [63]. Probably, this change in adsorption can be explained by the chemical structure of safranine T including positive charges and reactive amino groups. The loading pH of the model molecule was preferred as 6.8 due to the stability of multilayer integrity. At pH:6.8, safranine T is highly protonated and positively charged (dissociation constant, Ka:6.4) [72]. At this pH, the sulfonic acid groups of PSS are relatively dissociated and interact with the cationic dye molecule. On the other hand, PAA is a weak acid, and the carboxylic acid groups in its structure are sensitive to pH. The dissociation constant of PAA is 4.8 [73], and COOH groups become ionized COO^- under loading conditions. At the same time, reactive amino groups

Table 1 Safranine T loading and release% of the LbL multilayered films prepared from single/blend anionic PEs depending on blend composition and pH

LbL film	Safranine-T loading (24 h) mg/cm^2 (pH:6.8)	Safranine-T release % (~2 weeks) mg/cm^2 (pH:11)
$(PDADMAC/PAA)_{20}$	317.2	60
$(PDADMAC/PAA25PSS75)_{20}$	3960.8	40%
$(PDADMAC/PAA50PSS50)_{20}$	1098.8	90%
$(PDADMAC/PAA75PSS25)_{20}$	3419.8	67%
$(PDADMAC/PSS)_{20}$	435.5	24%

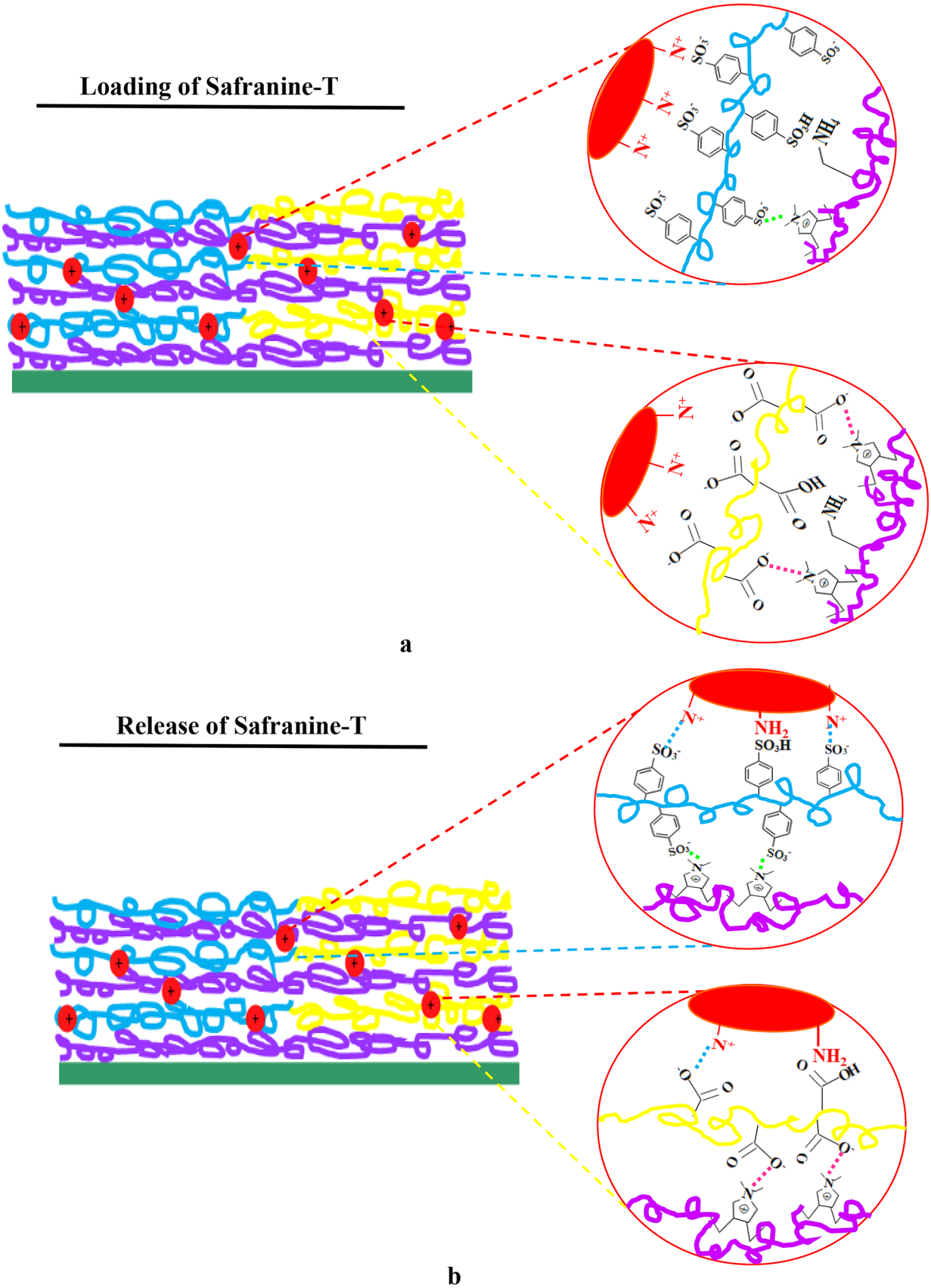

Scheme 2 Schematic representation of (**a**) safranine T loading at pH:6.8 and (**b**) safranine T release at pH:11

of safranine T are likely to react with unprotonated anionic PEs having carboxylic acid and sulfonic acid groups. In contrast to safranine T deposition through LbL films of single anionic PE, a larger amount of safranine T accumulation was observed for the multilayered films prepared from blend PEs. Among the blend structured LbL films, $(PDADMAC/PSS50PAA50)_{20}$ exhibited smaller safranine T adsorption. On the other hand, $(PDADMAC/PSS25PAA75)_{20}$ and $(PDADMAC/PSS75PAA25)_{20}$ had almost 3419.8 mg/cm^2 and 3960.8 mg/cm^2 cationic dye deposition, respectively. Higher safranine T adsorptions of PAA-rich and PSS-rich blend films can be explained as follows. At pH 6.8 where the loading was performed, unprotonated carboxylic acid groups of PAA in PAA-rich LbL blend film can react with amino groups of safranine T to form amide linkages. On the contrary, PSS-rich LbL blend film can interact with cationic dye by the reaction of unprotonated sulfonic acid groups of PSS and amino groups of safranine T. Furthermore, electrostatic interactions between opposite charges may take place even if PDADMAC and PSS were partly ionized at pH:6.8. Therefore, $(PDADMAC/PSS75PAA25)_{20}$ showed relatively larger deposition compared to $(PDADMAC/PSS25PAA75)_{20}$. Interestingly, it was found out that safranine T deposition of $(PDADMAC/PSS50PAA50)_{20}$ was lower than those of other LbL blend films of negatively charged PEs. In another word, safranine T accumulation of PAA-rich or PSS-rich blend LbL films was obviously larger than that of $(PDADMAC/PSS50PAA50)_{20}$. In summary, it can be stated that safranine T accumulation through the LbL films can be controlled depending on pH and blend composition of anionic PEs.

Release studies of the safranine T loaded LbL films were performed as explained in the experimental section, and safranine T release plots are presented in Fig. 3 as a function of time and blend composition of negatively charged PEs.

As one can see from Fig. 3, the highest desorption was observed for $(PDADMAC/PSS50PAA50)_{20}$ whereas $(PDADMAC/PSS)_{20}$ had the lowest safranine T release after almost 350 h. The lowest desorption of safranine T for $(PDADMAC/PSS)_{20}$ can be explained by the stronger interaction between $(PDADMAC/PSS)_{20}$ and safranine T at pH:11. As it was known from the literature [63, 71, 74, 75], $(PDADMAC/PAA)_{20}$ and $(PDADMAC/PSS)_{20}$ did not exhibit any multilayer degradation at basic conditions. Similar to our explanation mentioned above, not only the positive charges but also the functional amino groups of safranine T can interact with protonated and unprotonated sulfonic acid groups of PSS. Because of that, almost 24% safranine T release of $(PDADMAC/PSS)_{20}$ can be understandable. On the other hand, $(PDADMAC/PAA)_{20}$ displayed almost 60% of safranine T desorption. The remaining dye can be mainly attributed to the reaction of unprotonated carboxylic acid of PAA and amino groups of safranine T yielding amide

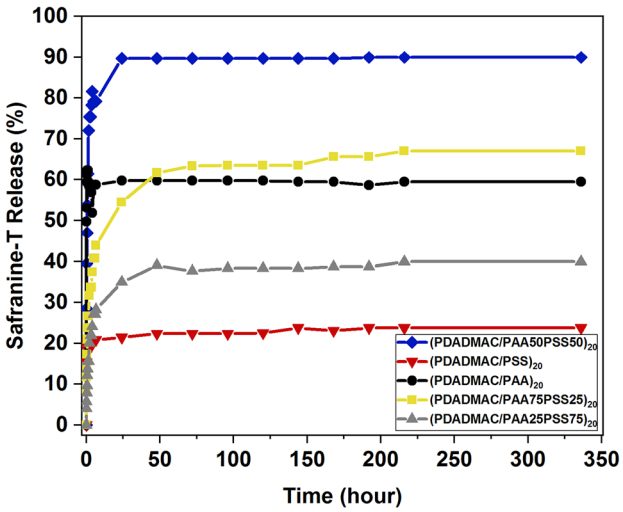

Fig. 3 Safranine-T release % of the LbL films prepared from single/blend anionic PEs in PBS as a function of time and blend composition at pH:11

linkages at pH 11. Amide linkages possibly formed by the reaction of unprotonated carboxylic acid groups (–COOH) of PAA and NH_2 groups of safranine T can lead to a blockage for dye release if PAA-rich blend composition was used in the feed solution for the preparation of multilayers. Almost 33% of entrapped safranine T can be explained by this phenomenon for $(PDADMAC/PAA75PSS25)_{20}$. Similar to $(PDADMAC/PSS)_{20}$, the lowest safranine T desorption was detected for PSS-rich blend film. This lower (40%) desorption of safranine T at basic condition can be explained by (i) ionic bonding with partial oppositely charged groups of PSS and quaternized ammonium of safranine T and (ii) hydrogen bonding between amino groups and sulfonic acid of PSS. If safranine T releases % of $(PDADMAC/PAA75PSS25)_{20}$ and $(PDADMAC/PAA25PSS75)_{20}$ were compared, it can be concluded that the relatively strong interactions between PSS and safranine T resulted in a higher dye entrapping through LbL film. Interestingly, the largest dye desorption was observed for $(PDADMAC/PAA50PSS50)_{20}$ and found to be roughly 90%. This might be explained by the removal of weakly bonded safranine T due to the reorganization of LbL film at pH:11[74, 75], and PAA becomes stiffer as the pH increases. Maybe another reason is the surface smoothness of the LbL films regardless of chemical composition. In our AFM measurements and in the literature [76, 77], it was mentioned that PAA had a coiled and loopy structure whereas PSS was relatively flat and less rough. On the other hand, reduced ionization degree of PSS and PAA can lead to weaken the electrostatic interactions between cationic dye and anionic polyelectrolytes at pH:11. By the way, it was observed that safranine T release% sharply increased within a couple of minutes and then remained almost the same at

pH 11. During the first 5 min, most of the adsorbed safranine T released for all prepared LbL films. Probably, this result can be explained by the changes in chemical interactions depending on pH as proposed in Scheme 2b.

Contact angle measurement

Surface wettability properties of the hydrophilized quartz glass and LbL multilayered films were determined after safranine T desorption. The related pictures are given in Fig. 4.

The average contact angle (θ_{ave}) value of the hydrophilized quartz glass was $86 \pm 1.2°$ while θ_{ave} of the dye desorbed $(PDADMAC/PAA)_{20}$, $(PDADMAC/PSS50PAA50)_{20}$, and $(PDADMAC/PSS)_{20}$ was found to be $41 \pm 2.2°$, $39 \pm 1.8°$, and $78 \pm 1.9°$, respectively. One can see from the figure that θ_{ave} of dye released $(PDADMAC/PSS)_{20}$ was higher than those of other LbL films obtained from single/blend anionic PEs. Even if more safranine T was entrapped inside the LbL film including single PSS, the bigger hydrophobicity of $(PDADMAC/PSS)_{20}$ can be explained by possible two reasons. Firstly, the hydrophobic character of aromatic groups of PSS existed in the LbL film, and the second one was the high root-mean-square (rms) value of the formed LbL film. Contrarily, dye desorbed $(PDADMAC/PAA)_{20}$ and $(PDADMAC/PSS50PAA50)_{20}$ showed obvious hydrophilic character, and their θ_{ave} values were almost the same. This result can be explained by the presence of PAA in the multilayer composition.

AFM

To evaluate and compare the surface topographies, AFM photos of the Safranin-T-released LbL films of single/blend negatively charged PEs are given in Fig. 5. One can see from the figure that the root-mean-square (rms) values were found to be 2.63 and 3.25 nm for $(PDADMAC/PAA)_{20}$ and $(PDADMAC/PSS50PAA50)_{20}$, respectively. This result showed the rms value of the LbL blend film increased by adding PSS to the PE feed composition whereas $(PDADMAC/PAA)_{20}$ film led to a lowering in

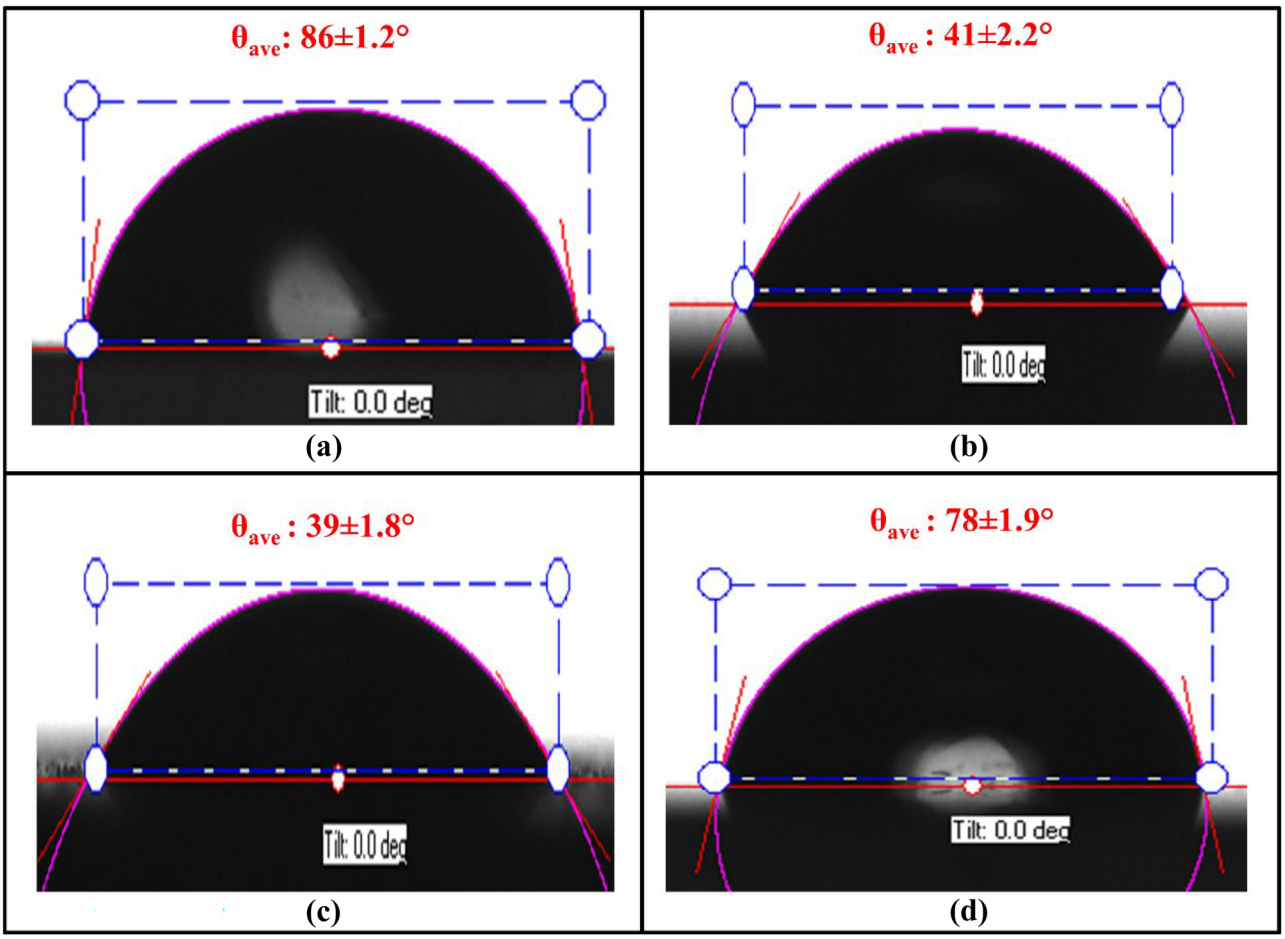

Fig. 4 Contact angle photos of (**a**) hydrophilized quartz glass and safranine T desorbed (**b**) $(PDADMAC/PAA)_{20}$, (**c**) $(PDADMAC/PSS50PAA50)_{20}$ and (**d**) $(PDADMAC/PSS)_{20}$ at pH 11

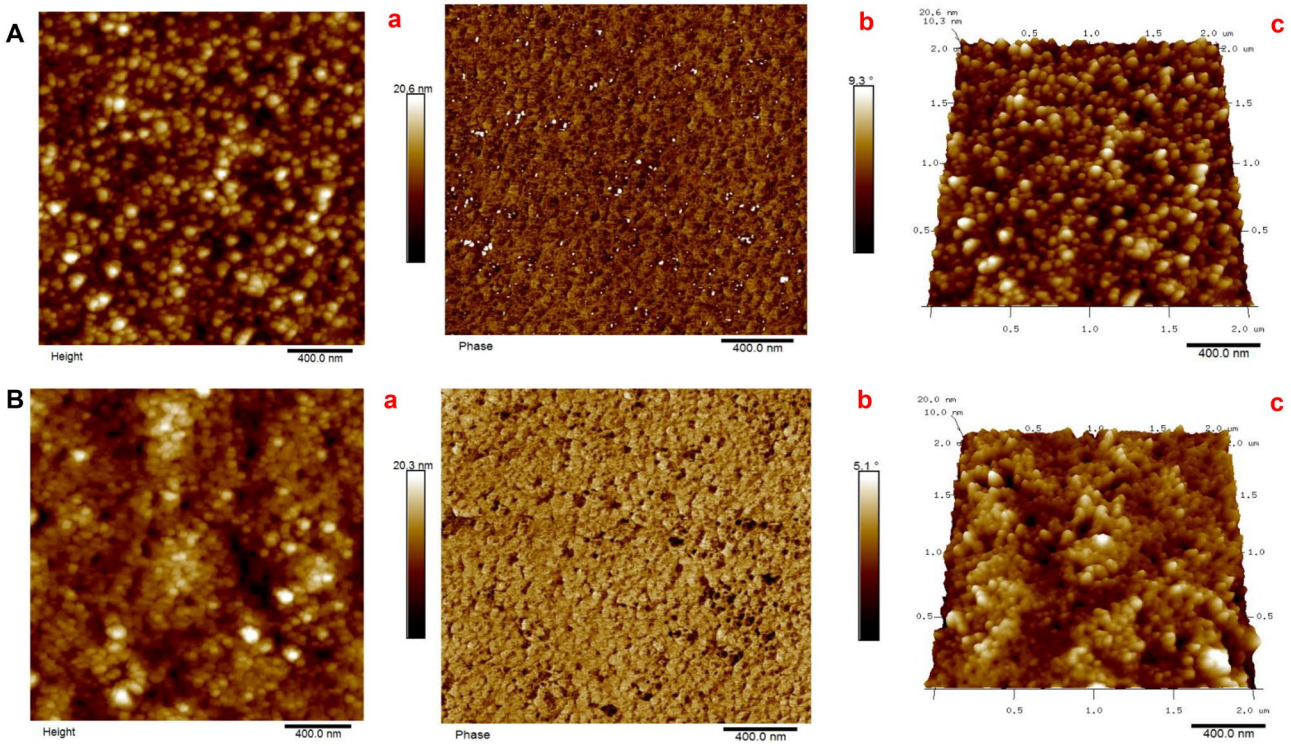

Fig. 5 AFM images of (**A**) safranine T released from $(PDADMAC/PAA)_{20}$, (**B**) safranine T released from $(PDADMAC/PSS50PAA50)_{20}$ and (a) phase, (b) height, (c) 3D-height AFM images

surface roughness. Probably, the use of PAA can lead to forming a flatter structure in $(PDADMAC/PAA)_{20}$ multilayers due to its partially recomposed chain conformational structure at pH:11. Considering that the entrapped safranine T amounts were almost the same for these films, it can be concluded that the roughness of LbL film prepared from single/blend anionic PEs strongly depends on their chemical structure.

Conclusions

In this study, sorption behavior of safranine T through the Layer-by-Layer (LbL) multilayered films of poly(diallyldimethylammonium chloride) (PDADMAC) and single/blend polyanions, namely, poly(acrylic acid) (PAA) and poly(styrenesulfonate) (PSS), are described. The growths of multilayered films and their safranine T sorption behavior are successfully monitored using UV–Vis spectroscopy in terms of blend ratio of anionic polyelectrolytes (PEs) and pH. The build-up of LbL multilayers on the quartz glass surface shows an increasing profile with the number of deposited bilayers. Dye loading and desorption properties of the LbL films of single/blend negatively charged PEs mainly depend on the interactions of PEs and safranine T. Strong interactions between PSS and safranine T result in a higher dye entrapping through the LbL films whereas either PAA-rich or single PAA-based LbL film exhibits larger dye desorption. A higher PSS content in the feed blend composition leads to an observable increase in θ_{ave} and surface roughness while the use of PAA can lead to forming a flatter surface due to its partially recomposed chain conformational structure at pH:11. In consequence, this study shows that LbL multilayers obtained from single and blend anionic PEs polyanions can be considered as an encouraging material platform for the controlled release of charged species such as protein, drug, and dye. because of their tunable physicochemical and morphological properties as well as surface wettability.

Funding The Scientific and Technological Research Council of Turkey (Grant 112M290) and Scientific Research Projects Coordination Unit of Istanbul University—Cerrahpaşa (Grant numbers 37682) provided the funding for this study.

Declarations

Competing interests The authors declare no competing interests.

References

1. Picart C, Caruso F, Voegel J-C (2015) Layer-by-layer films for biomedical applications. Wiley-VCH Verlag GmbH & Co. KGaA. https://doi.org/10.1002/9783527675869
2. Richardson JJ, Cui J, Björnmalm M et al (2016) Innovation in layer-by-layer assembly. Chem Rev 116:14828–14867. https://doi.org/10.1021/acs.chemrev.6b00627
3. Zhao S, Caruso F, Dahne L et al (2019) The future of layer-by-layer assembly: a tribute to ACS nano associate Editor Helmuth Mohwald. ACS Nano 13:6151–6169. https://doi.org/10.1021/acsnano.9b03326
4. Decher G, Hong J-D (1991) Buildup of ultrathin multilayer films by a self-assembly process, 1 consecutive adsorption of anionic and cationic bipolar amphiphiles on charged surfaces. https://doi.org/10.1002/masy.19910460145
5. Decher G, Hong JD, Schmitt J (1991) Buildup of ultrathin multilayer films by a self-assembly process: II. consecutively alternating adsorption of anionic and cationic polyelectrolytes on charged surfaces. Thin Solid Films 210–211:831–835. https://doi.org/10.1002/bbpc.19910951122
6. Decher G, Schlenoff JB (2012) Multilayer thin films: sequential assembly of nanocomposite materials, Second Edition, Second. Wiley-VCH, Germany
7. Alkekhia D, Hammond PT, Shukla A (2020). Layer-by-layer biomaterials for drug delivery. https://doi.org/10.1146/annurev-bioeng-060418
8. Ghiorghita CA, Bucatariu F, Dragan ES (2019) Influence of cross-linking in loading/release applications of polyelectrolyte multilayer assemblies. A review Mater Sci Eng C 105. https://doi.org/10.1016/j.msec.2019.110050
9. Antipov AA, Sukhorukov GB, Donath E, Mo H (2001). Sustained release properties of polyelectrolyte multilayer capsules. https://doi.org/10.1021/jp002184
10. Choi J, Rubner MF (2005) Influence of the degree of ionization on weak polyelectrolyte multilayer assembly. Macromolecules 38:116–124. https://doi.org/10.1021/ma048596o
11. Petrov AI, Antipov AA, Sukhorukov GB (2003) Base-acid equilibria in polyelectrolyte systems: from weak polyelectrolytes to interpolyelectrolyte complexes and multilayered polyelectrolyte shells. Macromolecules 36:10079–10086. https://doi.org/10.1021/ma034516p
12. Du P, Zhao X, Zeng J et al (2015) Layer-by-layer engineering fluorescent polyelectrolyte coated mesoporous silica nanoparticles as pH-sensitive nanocarriers for controlled release. Appl Surf Sci 345:90–98. https://doi.org/10.1016/j.apsusc.2015.03.151
13. Xie M, Zhang F, Liu L et al (2018) Surface modification of graphene oxide nanosheets by protamine sulfate/sodium alginate for anti-cancer drug delivery application. Appl Surf Sci 440:853–860. https://doi.org/10.1016/j.apsusc.2018.01.175
14. Kolasińska M, Warszyński P (2005) The effect of nature of polyions and treatment after deposition on wetting characteristics of polyelectrolyte multilayers. In: Applied Surface Science. Elsevier, pp 759–765. https://doi.org/10.1016/j.apsusc.2005.02.060
15. Deligöz H, Tieke B (2014) QCM-D study of layer-by-layer assembly of polyelectrolyte blend films and their drug loading-release behavior. Colloids Surfaces A Physicochem Eng Asp 441:725–736. https://doi.org/10.1016/j.colsurfa.2013.10.033
16. Crespilho FN, Zucolotto V, Brett CMA et al (2006) Enhanced charge transport and incorporation of redox mediators in layer-by-layer films containing PAMAM-encapsulated gold nanoparticles. J Phys Chem B 110:17478–17483. https://doi.org/10.1021/jp062098v
17. Seo J, Lutkenhaus JL, Kim J et al (2008) Effect of the layer-by-layer (LbL) deposition method on the surface morphology and wetting behavior of hydrophobically modified PEO and PAA LbL films. Langmuir 24:7995–8000. https://doi.org/10.1021/la800906x
18. Yu D, Dai L (2010) Self-assembled graphene/carbon nanotube hybrid films for supercapacitors. J Phys Chem Lett 1:467–470. https://doi.org/10.1021/jz9003137
19. Zhang M, Yan Y, Gong K et al (2004) Electrostatic layer-by-layer assembled carbon nanotube multilayer film and ıts electrocatalytic activity for O 2 reduction. Langmuir 20:8781–8785. https://doi.org/10.1021/la0489231
20. Caruso F, Lichtenfeld H, Donath E, Möhwald H (1999) Investigation of electrostatic interactions in polyelectrolyte multilayer films: binding of anionic fluorescent probes to layers assembled onto colloids. Macromolecules 32:2317–2328. https://doi.org/10.1021/ma980674i
21. Niu J, Shi F, Liu Z et al (2007) Reversible disulfide cross-linking in layer-by-layer films: preassembly enhanced loading and pH/reductant dually controllable release. Langmuir 23:6377–6384. https://doi.org/10.1021/la063670c
22. Volodkin D, Skirtach A, Möhwald H (2010) LbL films as reservoirs for bioactive molecules. Adv Polym Sci 240:135–161. https://doi.org/10.1007/12_2010_79
23. Richardson JJ, Björnmalm M, Caruso F (2015) Technology-driven layer-by-layer assembly of nanofilms. Science (80-.). 348. https://doi.org/10.1126/science.aaa2491.
24. Bag E, Begik O, Yusan P, Erel-Goktepe I (2015) Hydrogen-bonded multilayers with controllable pH-induced disintegration kinetics for controlled release applications from surfaces. J Macromol Sci Part A Pure Appl Chem 52:286–298. https://doi.org/10.1080/10601325.2015.1007274
25. Correa S, Dreaden EC, Gu L, Hammond PT (2016) Engineering nanolayered particles for modular drug delivery. J Control Release 240:364–386. https://doi.org/10.1016/j.jconrel.2016.01.040
26. Zhou J, Pishko MV, Lutkenhaus JL (2014) Thermoresponsive layer-by-layer assemblies for nanoparticle-based drug delivery. Langmuir 30:5903–5910. https://doi.org/10.1021/la501047m
27. Delcea M, Möhwald H, Skirtach AG (2011) Stimuli-responsive LbL capsules and nanoshells for drug delivery. Adv Drug Deliv Rev 63:730–747. https://doi.org/10.1016/j.addr.2011.03.010
28. Kurapati R, Groth TW, Raichur AM (2019) Recent developments in layer-by-layer technique for drug delivery applications. ACS Appl. Bio Mater. https://doi.org/10.1021/acsabm.9b00703
29. Wood KC, Boedicker JQ, Lynn DM, Hammond PT (2005) Tunable drug release from hydrolytically degradable layer-by-layer thin films. Langmuir 21:1603–1609. https://doi.org/10.1021/la0476480
30. Iost RM, Crespilho FN (2012) Layer-by-layer self-assembly and electrochemistry: applications in biosensing and bioelectronics. Biosens Bioelectron 31:1–10. https://doi.org/10.1016/j.bios.2011.10.040
31. Yut A, Caruso F (2003) Thin films of polyelectrolyte-encapsulated catalase microcrystals for biosensing. Anal Chem 75:3031–3037. https://doi.org/10.1021/ac0340049
32. Deshmukh PK, Ramani KP, Singh SS et al (2013) Stimuli-sensitive layer-by-layer (LbL) self-assembly systems: targeting and biosensory applications. J Control Release 166:294–306. https://doi.org/10.1016/j.jconrel.2012.12.033

33. Mariani S, Robbiano V, Strambini LM et al (2018) Layer-by-layer biofunctionalization of nanostructured porous silicon for high-sensitivity and high-selectivity label-free affinity biosensing. Nat Commun 9. https://doi.org/10.1038/s41467-018-07723-8
34. Hu M, Mi B (2013) Enabling graphene oxide nanosheets as water separation membranes. Environ Sci Technol 47:3715–3723. https://doi.org/10.1021/es400571g
35. Liu S, Montazami R, Liu Y et al (2010) Influence of the conductor network composites on the electromechanical performance of ionic polymer conductor network composite actuators. Sensors Actuators, A Phys 157:267–275. https://doi.org/10.1016/j.sna.2009.11.022
36. Liu S, Montazami R, Liu Y et al (2009) Layer-by-layer self-assembled conductor network composites in ionic polymer metal composite actuators with high strain response. Appl Phys Lett 95. https://doi.org/10.1063/1.3179554
37. Andre RS, Shimizu FM, Miyazaki CM et al (2017) Hybrid layer-by-layer (LbL) films of polyaniline, graphene oxide and zinc oxide to detect ammonia. Sensors Actuators, B Chem 238:795–801. https://doi.org/10.1016/j.snb.2016.07.099
38. Shen Y, Liu J, Jiang J et al (2003) Fabrication of a metalloporphyrin-polyoxometalate hybrid film by a layer-by-layer method and ıts catalysis for hydrogen evolution and dioxygen reduction. J Phys Chem B 107:9744–9748. https://doi.org/10.1021/jp035274y
39. Ferreira M, Fiorito PA, Oliveira ON, Córdoba De Torresi SI (2004) Enzyme-mediated amperometric biosensors prepared with the Layer-by-Layer (LbL) adsorption technique. Biosens Bioelectron 19:1611–1615. https://doi.org/10.1016/j.bios.2003.12.025
40. Lin HJ, Li T, Huang MH et al (2019) Modulating unidirectional charge transfer via in situ etching-accompanied layer-by-layer self-assembly toward multifarious photoredox catalysis. J Phys Chem C 123:28066–28080. https://doi.org/10.1021/acs.jpcc.9b08738
41. Shin SR, Aghaei-Ghareh-Bolagh B, Gao X et al (2014) Layer-by-layer assembly of 3D tissue constructs with functionalized graphene. Adv Funct Mater 24:6136–6144. https://doi.org/10.1002/adfm.201401300
42. Kim K, Ryu JH, Lee DY, Lee H (2013) Bio-inspired catechol conjugation converts water-insoluble chitosan into a highly water-soluble, adhesive chitosan derivative for hydrogels and LbL assembly. Biomater Sci 1:783–790. https://doi.org/10.1039/c3bm00004d
43. Tang Z, Wang Y, Podsiadlo P, Kotov NA (2006) Biomedical applications of layer-by-layer assembly: From biomimetics to tissue engineering. Adv Mater 18:3203–3224. https://doi.org/10.1002/adma.200600113
44. Min J, Choi KY, Dreaden EC et al (2016) Designer dual therapy nanolayered ımplant coatings eradicate biofilms and accelerate bone tissue repair. ACS Nano 10:4441–4450. https://doi.org/10.1021/acsnano.6b00087
45. Cheng G, Yin C, Tu H et al (2019) Controlled co-delivery of growth factors through layer-by-layer assembly of core shell nanofibers for ımproving bone regeneration. ACS Nano 13:6372–6382. https://doi.org/10.1021/acsnano.8b06032
46. Ma W, Zhang Y, Li F et al (2019) Layer-by-layer assembly and electrochemical study of Alizarin Red S-based thin films. Polymers (Basel) 11. https://doi.org/10.3390/polym11010165
47. Jiang S, Chen X, Liu M (2004) The pH stimulated reversible loading and release of a cationic dye in a layer-by-layer assembled DNA/PAH film. J Colloid Interface Sci 277:396–403. https://doi.org/10.1016/j.jcis.2004.04.008
48. Şenel M, Ebru Koç F (2020) Controlled release of methylene blue from layer-by-layer assembled chitosan/polyacrylic acid. Int J Polym Mater Polym Biomater 69:258–262. https://doi.org/10.1080/00914037.2018.1563082
49. Wang B, Gao C, Liu L (2005) Loading and release behaviors of compressed polyelectrolyte multilayers for small dye molecules. J Phys Chem B 109:4887–4892. https://doi.org/10.1021/jp0450282
50. Schneider G, Decher G, Nerambourg N et al (2006) Distance-dependent fluorescence quenching on gold nanoparticles ensheathed with layer-by-layer assembled polyelectrolytes. Nano Lett 6:530–536. https://doi.org/10.1021/nl052441s
51. Ghosh I, Das B, Nath RK et al (2016) Spectroscopic characterization of Niagara blue dye in the restricted geometry of layer-by-layer self-assembled films. Surf Rev Lett 23. https://doi.org/10.1142/S0218625X16500566
52. Nath J, Deb S, Bhattacharjee D, Nath RK (2011) Formation and characterization of anionic dye-polycation molecular films by layer-by-layer adsorption process. Mol Cryst Liq Cryst 548:96–106. https://doi.org/10.1080/15421406.2011.590371
53. Ding C, Xu S, Lin J et al (2012) Controlled loading and release of methylene blue for hydrogen-bonded LbL poly(vinyl pyrrolidone)/poly (acrylic acid) film. J Polym Res 19. https://doi.org/10.1007/s10965-011-9817-x
54. Ding C, Xu S, Wang J et al (2012) Controlled loading and release of methylene blue in layer-by-layer assembled polyelectrolyte films. Mater Sci Eng C 32:670–673. https://doi.org/10.1016/j.msec.2012.01.005
55. Gu R, Yuan X, Wu R et al (2014) Layer-by-layer assembled hydrogel nanocomposite film with a high loading capacity. J Appl Polym Sci 131. https://doi.org/10.1002/app.39352
56. Tedeschi C, Caruso F, Möhwald H, Kirstein S (2000) Adsorption and desorption behavior of an anionic pyrene chromophore in sequentially deposited polyelectrolyte-dye thin films. J Am Chem Soc 122:5841–5848. https://doi.org/10.1021/ja994029i
57. Vidyasagar A, Sung C, Losensky K, Lutkenhaus JL (2012) PH-dependent thermal transitions in hydrated layer-by-layer assemblies containing weak polyelectrolytes. Macromolecules 45:9169–9176. https://doi.org/10.1021/ma3020454
58. Lundin M, Solaqa F, Thormann E et al (2011) Layer-by-layer assemblies of chitosan and heparin: Effect of solution ionic strength and pH. Langmuir 27:7537–7548. https://doi.org/10.1021/la200441u
59. Vidyasagar A, Sung C, Gamble R, Lutkenhaus JL (2012) Thermal transitions in dry and hydrated layer-by-layer assemblies exhibiting linear and exponential growth. ACS Nano 6:6174–6184. https://doi.org/10.1021/nn301526b
60. Sung C, Vidyasagar A, Hearn K, Lutkenhaus JL (2012) Effect of thickness on the thermal properties of hydrogen-bonded LbL assemblies. Langmuir 28:8100–8109. https://doi.org/10.1021/la301300h
61. Dreaden EC, Morton SW, Shopsowitz KE et al (2014) Bimodal tumor-targeting from microenvironment responsive hyaluronan layer-by-layer (LbL) nanoparticles. ACS Nano 8:8374–8382. https://doi.org/10.1021/nn502861t
62. Ding C, Xu S, Wang J et al (2012) Controlled loading and release of methylene blue from LbL polyurethane/poly(acrylic acid) film. Polym Adv Technol 23:1283–1286. https://doi.org/10.1002/pat.2044
63. Yılmaz Aykut D, Yolaçan Ö, Deligöz H (2020) pH stimuli drug loading/release platforms from LbL single/blend films: QCM-D and in-vitro studies. Colloids Surfaces A Physicochem Eng Asp 602:125113. https://doi.org/10.1016/j.colsurfa.2020.125113
64. Ergün A, Tümer EH, Cengiz HY, Deligöz H (2020) Monitoring the salt stability of layer-by-layer self-assembled films from polyelectrolyte blends by quartz crystal microbalance-dissipation and their ıon separation performances. Polym Eng Sci. https://doi.org/10.1002/pen.25356
65. Arslan M, Dönmez G, Ergün A et al (2020) Preparation, characterization, and separation performances of novel surface modified LbL composite membranes from polyelectrolyte blends and MWCNT. Polym Eng Sci 60:341–351. https://doi.org/10.1002/pen.25289
66. Deniz M, Deligöz H (2019) Flexible self-assembled polyelectrolyte thin films based on conjugated polymer: quartz cristal

microbalance dissipation (QCM-D) and cyclic voltammetry analysis. Colloids Surfaces A Physicochem Eng Asp 563:206–216. https://doi.org/10.1016/j.colsurfa.2018.12.014
67. Quinn A, Tjipto E, Yu A et al (2007) Polyelectrolyte blend multilayer films: surface morphology, wettability, and protein adsorption characteristics. Langmuir 23:4944–4949. https://doi.org/10.1021/la0634746
68. Liu L, Pan Y, Zhao Y et al (2020) Self-assembly of phosphonate-metal complex for superhydrophobic and durable flame-retardant polyester–cotton fabrics. Cellulose 27:6011–6025. https://doi.org/10.1007/s10570-020-03148-z
69. Ospanova A, Savdenbekova B, Kubasheva Z et al (2020) Several features of producing polyelectrolyte-based nanolayers by the multi-layer assembly. Mater Today Proc 31:584–587. https://doi.org/10.1016/j.matpr.2020.07.070
70. Ramos JJI, Llarena I, Moya SE (2011) Unusual collapse of highly hydrated polyelectrolyte multilayers with the ionic strength. J Polym Sci Part A Polym Chem 49:2346–2352. https://doi.org/10.1002/pola.24662
71. Han L, Mao Z, Wuliyasu H et al (2012) Modulating the structure and properties of poly(sodium 4-styrenesulfonate)/poly(diallyldimethylammonium chloride) multilayers with concentrated salt solutions. Langmuir 28:193–199. https://doi.org/10.1021/la2040533
72. Wang Y, Lin C, Wang Z et al (2019) Magnetic hollow poly(cyclotriphosphazene-co-4,4′-sulfonyldiphenol)-Fe3O4 hybrid nanocapsules for adsorbing Safranine T and catalytic oxidation of 3,3′,5,5′-tetramethylbenzidine. J Colloid Interface Sci 556:278–291. https://doi.org/10.1016/j.jcis.2019.08.073
73. Gopalakrishnan A, Mathew ML, Chandran J et al (2015) Sustainable polyelectrolyte multilayer surfaces: possible matrix for salt/dye separation. ACS Appl Mater Interfaces 7:3699–3707. https://doi.org/10.1021/am508298d
74. Iturri Ramos JJ, Stahl S, Richter RP, Moya SE (2010) Water content and buildup of poly(diallyldimethylammonium chloride)/poly(sodium 4-styrenesulfonate) and poly(allylamine hydrochloride)/poly(sodium 4-styrenesulfonate) polyelectrolyte multilayers studied by an in situ combination of a quartz crystal microb. Macromolecules 43:9063–9070. https://doi.org/10.1021/ma1015984
75. Alonso T, Irigoyen J, Iturri JJ et al (2013) Study of the multilayer assembly and complex formation of poly(diallyldimethylammonium chloride) (PDADMAC) and poly(acrylic acid) (PAA) as a function of pH. Soft Matter 9:1920–1928. https://doi.org/10.1039/c2sm26884a
76. Quinn A, Such GK, Quinn JF, Caruso F (2008) Polyelectrolyte blend multilayers: a versatile route to engineering interfaces and films. Adv Funct Mater 18:17–26. https://doi.org/10.1002/adfm.200700472
77. Slavgorodska M, Kyrychenko A (2020) Structure and dynamics of pyrene-labeled poly(Acrylic acid): Molecular dynamics simulation study. Chem Chem Technol 14:76–80. https://doi.org/10.23939/chcht14.01.076

Publisher's Note Springer Nature remains neutral with regard to jurisdictional claims in published maps and institutional affiliations.